

OPEN ACCESS

Imaging Cycle-Induced Damage of MnO₂ Microparticles

To cite this article: Stevie N. Bush et al 2020 J. Electrochem. Soc. 167 132501

View the article online for updates and enhancements.

You may also like

- Synthesis of -MnO₂/Reduced Graphene Oxide Hybrid In Situ and Application in Mq-Air Battery

Hui Liu, Jiaxi Zhang, Hongjie Fang et al.

 Sodium Charge Storage in Thin Films of MnO₂ Derived by Electrochemical Oxidation of MnO Atomic Layer Deposition Films

Matthias J. Young, Markus Neuber, Andrew C. Cavanagh et al.

- Rational design of flower-like MnO₂/Ti₂C₂T_x composite electrode for high performance supercapacitors Chenji Xia, Yijia Luo, Xiaoqing Bin et al.

Investigate your battery materials under defined force! The new PAT-Cell-Force, especially suitable for solid-state electrolytes!



- Battery test cell for force adjustment and measurement,
 0 to 1500 Newton (0-5.9 MPa at 18mm electrode diameter)
- Additional monitoring of gas pressure and temperature

www.el-cell.com +49 (0) 40 79012 737 sales@el-cell.com







Imaging Cycle-Induced Damage of MnO₂ Microparticles

Stevie N. Bush,* Duliette Experton, Anais Teyssendier de La Serve, Emily P. Johnson, and Charles R. Martin**,z

Department of Chemistry, University of Florida, Gainesville, Florida 32611-7200, United States of America

 MnO_2 has been proposed as an electrode material in electrochemical energy storage devices. However, poor cycle life, especially in aqueous electrolytes, remains a detriment to commercialization. Prior studies have suggested a number of explanations for this capacity loss; however, experiments aimed at elucidating the details of the degradation process (es) are sparse. We describe here a microtube-membrane construct that allows for electrodeposition of monodisperse MnO_2 microparticles distributed across the membrane surface, and for subsequent electrochemical cycling of these MnO_2 particles. This allowed for a detailed analysis of the effect of cycling on the MnO_2 , by simply imaging the membrane surface before and after cycling. When an aqueous electrolyte was used, gross changes in particle shape, size and morphology were observed over the course of 500 cycles. Partial dissolution occurred as well. No such changes were observed when the MnO_2 particles were cycled (up to 500 times) in a propylene carbonate electrolyte solution.

© 2020 The Author(s). Published on behalf of The Electrochemical Society by IOP Publishing Limited. This is an open access article distributed under the terms of the Creative Commons Attribution 4.0 License (CC BY, http://creativecommons.org/licenses/by/4.0/), which permits unrestricted reuse of the work in any medium, provided the original work is properly cited. [DOI: 10.1149/1945-7111/abb7ed]

Manuscript submitted June 2, 2020; revised manuscript received August 30, 2020. Published September 18, 2020.

Supplementary material for this article is available online

There is considerable interest in developing MnO_2 as an electrode material in electrochemical energy-storage devices, ^{1,2} such as pseudocapacitors^{3–5} and lithium-ion batteries. ^{6–8} In these applications energy is typically stored and released by a reversible redox reaction involving cations from the contacting electrolyte solution. Assuming the cation is ${\rm Li}^+$, this half reaction can be written as, ^{9–12}

$$MnO_2 + Li^+ + e^- \leftrightarrow LiMnO_2$$
 [1]

with standard reduction potential of $-0.13\,V$ vs NHE. A recent review on the application of MnO_2 to supercapacitors has pointed out that further development will require improvements in energy density, structural stability, and cycle life. Since cycle life is related to structural and chemical stability it is important to understand the mechanism by which cycling-induced (Eq. 1) degradation of MnO_2 occurs. In spite of the practical importance of understanding degradation, reports detailing the structural and chemical changes during cycling of MnO_2 are sparse $^{11,13-20}$

We describe here a membrane-based construct for the electrochemical synthesis of discrete and monodisperse MnO₂ microparticles that are fixed to specific places on the membrane surface. This was accomplished using a gold-microtube membrane, where the microtubes act as electrodes for electrodeposition and cycling of the MnO₂ microparticles (Fig. 1). By imaging the membrane surface after cycling, the changes in particle shape, size and morphology can be monitored. This was accomplished, here, using scanning electron microscopy (SEM). The images showed that, when cycled in in aqueous LiClO₄, the MnO₂ microparticles became larger, and adopted a coarser morphology. Ultimately, after 500 cycles, the particles were diffuse, dispersed over a larger area, and highly dendritic. The images suggested that partial dissolution of the MnO₂ occurred. This was confirmed by chemical analysis of the electrolyte after cycling. In contrast, analogous cycling in propylene carbonate caused no change in particle size, shape, or morphology after 500 cycles.

Experimental

Materials.—Anhydrous SnCl₂, Na₂SO₃, NaHCO₃, AgNO₃, LiClO₄ and Mn(CH₃COO)₂ were purchased from Sigma-Aldrich. Commercial gold plating solution (Oromerse Part B) was obtained from Technic, Inc. Purified water was prepared by passing house-distilled water through a Barnstead E-pure model D4641 water purification system. All other chemicals were of reagent grade and were used as received from Fisher Scientific.

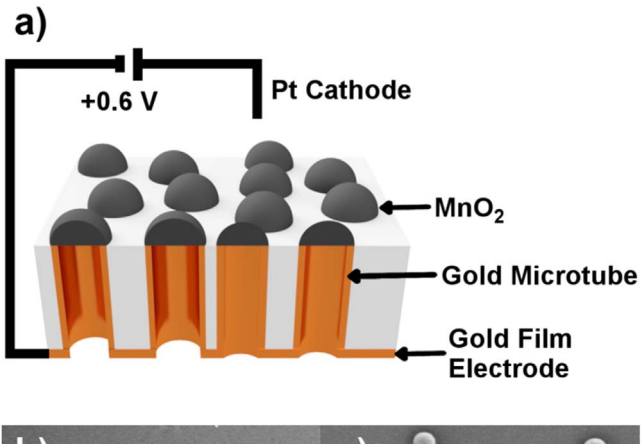
Preparation of the gold-microtube membranes.—The method used to prepare the gold-microtube membranes has been described in detail previously. $^{21-25}$ Briefly, ion-tracked polyethylene terephthalate (PET) membranes (12 μm thick) were obtained from GSI (Darmstadt, Germany). Chemical etching 26,27 was used to prepare 800 nm diameter pores in these membranes. An electroless plating procedure 22,28 was then used to deposit gold microtubes in the pores of the PET membranes (Fig. 1). In addition to the gold microtubes lining the pore walls, the electroless plating method yielded thin (\sim 100 nm) gold surface films on both faces of the membrane. 25,28 A piece of copper tape (3MT) was attached to one of the gold surface films (lower in Fig. 1a) to make electrical contact to the gold microtubes within the pores. 28,29 The other gold surface film was removed by scrubbing the surface with a cotton swab wetted with ethanol 21,28 to expose the ends of the gold microtubes where the MnO₂ particles were deposited (Fig. 1a).

Electrosynthesis of the MnO_2 microparticles.—Electrochemical synthesis of MnO_2 by oxidation of Mn^{2+} solutions is well known. $^{30-32}$ Aqueous solutions 50 mM in manganese acetate and 0.1 M in sodium sulfate were used here. 21,33,34 The gold-microtube membrane was mounted in a U-tube cell 25,35 with this manganese solution in the half-cell facing the open gold microtubes (up in Fig. 1a). The other half-cell was filled with 0.1 M Na_2SO_4 . As illustrated in Fig. 1a, the gold microtubes are connected in parallel to the remaining (lower) gold surface film. A voltage of 0.6 V was applied to the microtubes relative to a Pt wire quasi-reference electrode (Pt_{qr}) also immersed in the manganese solution. This resulted in the oxidation of Mn^{2+} and deposition of monodisperse hemispherical MnO_2 particles at the open ends of the gold microtubes (Fig. 1c). Unless otherwise noted, a deposition time of 5 min was used. The voltage of the Pt_{qr} was measured vs an Ag/AgCl reference electrode (RE-5B from BASi). A stable value of 0.28 ± 0.01 V (vs Ag/AgCl) was obtained. This makes the voltage used to

^{*}Electrochemical Society Student Member.

^{**}Electrochemical Society Fellow.

^zE-mail: crmartin@chem.ufl.edu



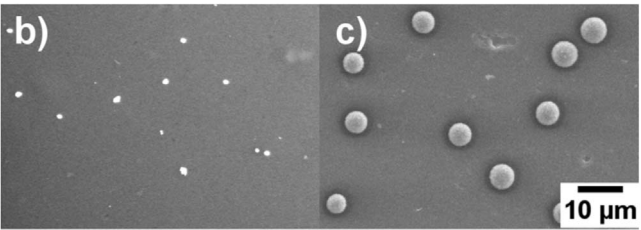


Figure 1. (a) Schematic representation of the gold microtube membrane with electrodeposited MnO_2 particles at the open mouths of gold microtubes. The underlying gold film acts as the anode during electrodeposition. Dimensions are not to scale. (b) Scanning electron micrograph of the surface of a gold-microtube membrane. The white spots are the open mouths of the gold microtubes. (c) Scanning electron micrograph of the membrane surface after electrodeposition of the MnO_2 particles.

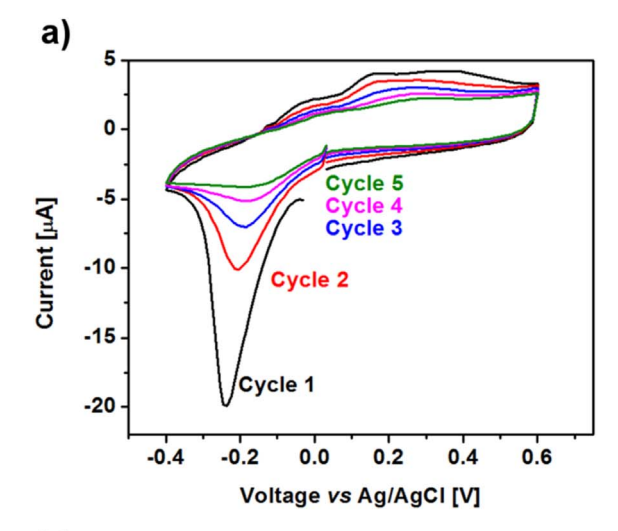
conduct the electrosynthesis 0.88 V vs Ag/AgCl. All voltages reported henceforth are vs an Ag/AgCl reference.

X-ray photoelectron spectroscopy (XPS).—A Perkin Elmer 5100 XPS System equipped with an Al monochromatic source (50 W, 200 μ A, takeoff angle 45°) was used to study the surface composition of the MnO₂ particles. Data were obtained on membranes before and after deposition. Data analysis was performed using the PHI XPS software.

Cyclic voltammetry.—Cyclic voltammetry was conducted on thin films of MnO_2 electrodeposited across the surface of the gold microtube membrane. Thin films, as opposed to microparticles, were obtained because both gold surface layers were left intact. This resulted in deposition of a thin film of MnO_2 covering the exposed gold surface layer. Cyclic voltammograms were obtained in both aqueous $LiClO_4$ (0.1 M) and $LiClO_4$ in propylene carbonate (1 M) (Fig. 2).

Cycling induced changes in the MnO₂ particles.—Cycling was accomplished in the U-tube cell with both half-cells filled with 0.1 M LiClO₄. The particles were cycled by applying a voltage of 0.88 V for 1 min, a voltage of -0.12 V for 1 min, and then returning to 0.88 V for 1 min. Up to 500 such cycles were applied. SEM images of the membrane after various numbers of cycles were used to monitor the changes in the particles upon cycling. Particles cycled in both aqueous and propylene carbonate solutions were imaged. Electron micrographs were obtained using a Hitachi SU5000 Schottky Field-Emission Microscope. ImageJ software was used to obtain the diameters and density of the gold microtubes and the MnO₂ particles. The averages and standard deviations were determined using approximately 100 measurements from different images.

In addition, inductively couple plasma—atomic emission spectroscopy (ICP-AES) was used to detect and quantify Mn dissolved from the particles with repeated cycling in the aqueous solution.



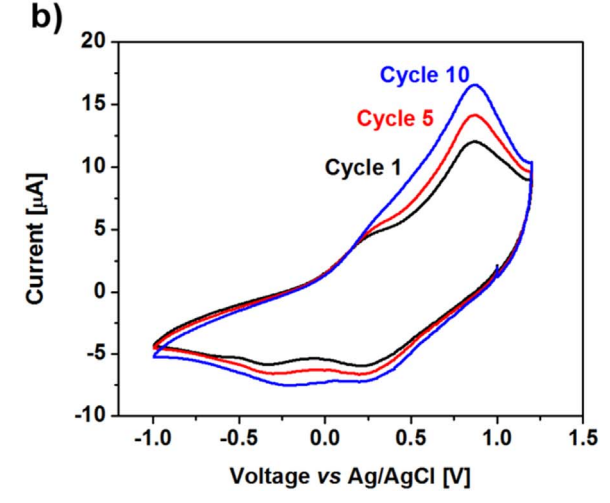


Figure 2. Cyclic voltammograms of the MnO $_2$ microparticles on the gold-microtube membrane measured in (a) aqueous of 0.1 M LiClO $_4$, and (b) 1 M LiClO $_4$ in propylene carbonate. The scan rate was 10 mV s $^{-1}$ in both cases.

ICP-AES analyses were accomplished with a Varian Vista RL CCD Simultaneous ICP-AES. The quantity of Mn dissolved in the electrolyte solution (aqueous 0.1 M LiClO₄) was measured after 100 and 500 cycles. Details of this analysis can be found in the Supplemental Material is available online at stacks.iop.org/JES/167/132501/mmedia.

Results and Discussion

Characteristics of the membrane, microtubes, and MnO_2 microparticles.—The gold microtube membranes were prepared by electroless plating of gold along the pore walls in a porous polymeric host (Fig. 1). $^{21-25}$ A recent review describes such membranes in detail. 25 The polymeric host membrane contained monodisperse 800 nm diameter pores, making the outside diameter of the gold microtubes 800 nm. Electron micrographs like those shown in Fig. 1b were used to determine the inside diameter of the tubes $(600 \pm 80 \text{ nm})$ and the number of tubes per cm² of membrane area $(1.9 \pm 0.8 \times 10^5 \text{ cm}^{-2})$. The tube walls were $\sim 100 \text{ nm}$ thick. In addition to the gold tubes, both membrane faces were coated with a thin $(\sim 100 \text{ nm})$ gold film. One film was removed prior to MnO₂ electrosynthesis. The other gold film was left intact and was used to make electrical contact with the microtubes (Fig. 1a).

The MnO_2 microparticles were synthesized electrochemically from aqueous solutions of $Mn^{2+30-32}$ The gold film (down in Fig. 1a) served as the anode during electrodeposition. Electrodeposition yielded MnO_2 microparticles at the open ends of

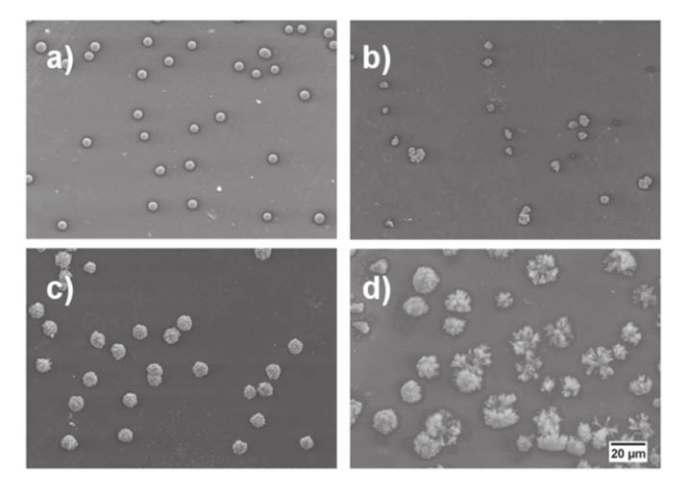


Figure 3. Electron micrographs of the surface of microtube/MnO₂ composite membranes (a) immediately after electrodeposition, and after (b) 100, (c) 300, and (d) 500 cycles in aqueous 0.1 M LiClO₄.

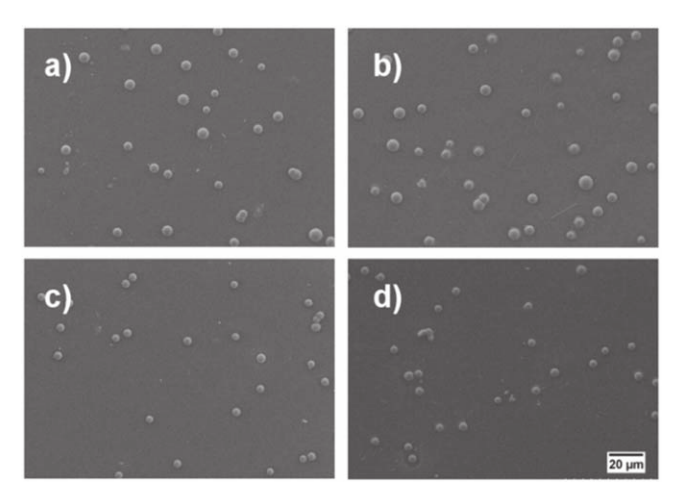


Figure 4. Electron micrographs of the surface of microtube/MnO₂ composite membranes a) after electrodeposition, and after (a) 100, (b) 300, and (c) 500 cycles in 0.1 M LiClO₄ in propylene carbonate.

the gold microtubes (Fig. 1c). The MnO_2 particle density was $1.3 \pm 0.2 \times 10^5 \, \mathrm{cm}^{-2}$, within experimental error identical to the gold microtube density. This indicated that a MnO_2 particle had been deposited at the mouth of each tube. After 5 min of deposition time the MnO_2 particles were $5 \pm 1 \, \mu \mathrm{m}$ in diameter (Fig. 1c).

As per our prior work on MnO_2 particles synthesized by a bipolar electrochemical method, ²¹ X-ray photoelectron spectroscopy (XPS) was used to determine the oxidation state of the as-synthesized MnO_2 . The XPS method is well known and has been described in detail. ^{36,37} Because of this prior work, the XPS data obtained for the MnO_2 particles prepared here are presented in the Supplemental materials. These data indicate that, as is typically the case for electrochemically synthesized MnO_2 , ^{32,38} a mixed valence material, approximately 90% Mn(IV) and 10% Mn(III), was obtained.

Cyclic voltammetry.—Cyclic voltammetry was used to confirm that the MnO_2 produced here showed electroactivity similar to previous examples of electrodeposited MnO_2 . ^{39–42} Cyclic voltammetry was conducted on electrodeposited thin films rather than on the MnO_2 microparticles. This is because during microparticle synthesis, MnO_2 does not deposit inside the gold microtubes²¹ and the tubes fill with electrolyte solution. This makes the capacitance and resistance of the gold-microtube membrane high. ^{25,28} As a result, when cyclic voltammetry was done on the MnO_2 particles

supported on the gold-microtube membrane, large sloping background currents were obtained obscuring the MnO_2 electrochemistry. By leaving both surface layers intact, a thin film of MnO_2 is deposited across the exposed gold surface layer (see Experimental). This film seals off the underlying microtubes, and the MnO_2 electrochemistry is not obscured (Fig. 2).

electrochemistry is not obscured (Fig. 2).

As per prior voltammetric studies, ^{39–42} when cycled in 0.1 M aqueous LiClO₄, the MnO₂ prepared here showed a large reduction peak at –240 mV, followed by a smaller set of oxidation peaks at about 30, 150 and 360 mV (Fig. 2a). The fade in capacity is clearly shown by the decrease in current with cycle number. This is especially noticeable for the cathodic peak at –240 mV. In contrast, no loss in capacity (over this limited cycle range) was observed when cycling was done in 1 M LiClO₄ in propylene carbonate (Fig. 2b). Indeed, as has been observed previously in this electrolyte, capacity increased over the first 10 cycles. ^{43–45}

Cycling induced degradation and dissolution.—SEM images of the membrane surface after 100, 300 and 500 cycles in aqueous 0.1 M LiClO₄ are shown in Fig. 3. Dramatic changes in particle shape, size and morphology were observed. Specifically, cycling caused the particles to become larger and to adopt a coarser morphology. Ultimately after 500 cycles, the particles were diffuse, dispersed over a larger area, and highly dendritic. To our knowledge, such changes in MnO₂ particle size, shape and morphology upon cycling have not been described previously. The ability to follow the fate of the particles upon cycling is greatly enhanced by the microtube membrane constructed described here.

Prior studies have suggested that capacity fading in MnO_2 is a result of partial dissolution of the reduced Mn(III) form of the material. 13,14,16,46 The dissolution reactions proposed entail acid-induced disproportionation of the solid Mn(III) into solid MnO_2 plus soluble Mn^{2+} . 14,16 For example, this reaction can be written as,

$$2\text{LiMnO}_2 + 4\text{H}^+ \rightarrow \text{MnO}_{2(s)} + \text{Mn}_{(aq)}^{2+} + 2\text{Li}^+ + 2\text{H}_2\text{O}$$
 [2]

The changes in particle morphology upon cycling observed here support the conclusion that partial dissolution has occurred upon cycling of the MnO₂ microparticles. Spectrophotometric analyses of the electrolyte were used to confirm that cycling in water causes partial dissolution of the MnO₂ particles. After 100 cycles, 3.4 \times 10⁻⁹ moles of Mn were present in the electrolyte solution; 4.8 \times 10⁻⁹ moles were present after 500 cycles. Assuming an initial particle diameter of 5 μ m and a MnO₂ density of 5 g per cm³, this corresponds to 48% and 66% of the MnO₂ present in the assynthesized particles.

However, the highly dendritic structures obtained after 500 cycles (Fig. 3d) indicate that some fraction of the Mn(II) liberated into the solution is being redeposited. This redeposited material could be MnO₂, resulting from the reoxidation of the soluble Mn(II) back to Mn(IV) during a positive cycle. In contrast, the redeposited material might be metallic Mn, resulting from the reduction of the soluble Mn(II) to Mn(0) during a negative cycle. That most of the material in our experiment is re-deposited at points far removed from the underlying gold microtube indicates that redeposition is occurring on the dendrites themselves; i.e., the redeposited material is acting as an electrode for further redeposition. We suggest that in order for this to occur, the redeposited material must be electronically conductive. This suggests that the redeposited material is metallic Mn(0), a conductor, and not MnO₂, which has a conductivity of only about 10^{-5} S cm⁻¹. ^{47,48}

That the redeposited material in our experiments is metallic Mn is supported by two other lines of investigation. First, deposition of metallic Mn, from soluble Mn²⁺, has been observed at the negative electrode in the battery application of MnO₂. ¹⁴ Second, the dendritic structures obtained here are reminiscent of the dendrites observed when electroplating certain metals such as Li. ^{49,50} In that case, the rate of deposition is nucleation limited, and dendritic growth occurs from the sparse number of nuclei obtained. ^{51,52} Again, this

necessitates that the deposited material is an electronic conductor. However, further study will be required to confirm that metallic Mn is present in the redeposited material.

In contrast to the aqueous electrolyte, particles cycled in 1 M LiClO₄ in propylene carbonate showed no change in size, shape or morphology over 500 cycles (Fig. 4). In particular, the particle diameter did not change with cycling with all particles having a diameter of $5 \pm 1 \mu m$ before and after cycling. This cycling stability over hundreds of cycles in propylene carbonate has been previously reported.⁵³ This supports the conclusion that dissolution is acidinduced, since the requisite hydronium ions are not present in propylene carbonate. 14,1

Conclusions

We have described here a gold-microtube-membrane construct for the electrochemical synthesis of discrete and monodisperse MnO₂ microparticles. The particles are deposited at the open ends of the gold microtubes, and a key advantage of this construct is that the membrane surface can be imaged to explore the fate of the particles upon cycling. The images obtained showed that gross changes in particle shape, size and morphology occurred upon cycling the MnO₂ particles in aqueous electrolyte. Detailed studies of this type have not been previously reported for cycle-induced degradation of MnO₂.

We have also shown that partial dissolution of the MnO₂ particles occurred during cycling in aqueous solution and have quantified the amount of dissolved Mn. In addition, the images show that some redeposition occurs during cycling. The data obtained here, and by others, indicate that the redeposited material is electronically conductive metallic Mn. 14,16 In contrast, cycling in propylene carbonate caused no change in particle size, shape and morphology up to 500 cycles.

As noted above, it has been proposed that the Mn liberated into the solution during cycling results from acid-induced disproportionation of the electrochemically produced Mn(III) into MnO₂ and soluble Mn²⁺. 14,16 The gold microtube membrane construct described here could act as a convenient vehicle for studying the decomposition mechanism. If acid-induced disproportionation is, indeed, occurring, then the cycling induced damage observed in Fig. 3 should be mitigated by using higher pH solutions during cycling. Finally, it is worth pointing out that this microtubemembrane construct could be used to conduct analogous experiments on any electrode material that can be electrochemically synthesized.

Acknowledgments

This work was supported by the Nanostructures for Electrical Energy Storage (NEES), an Energy Frontier Research Center funded by the U.S. Department of Energy, Office of Science, and Basic Energy Sciences under award number DESC0001160. Juliette Experton also acknowledges the 2018 Eastman Summer Fellowship and the ACS Division of Analytical Chemistry Fellowship.

ORCID

Stevie N. Bush https://orcid.org/0000-0002-0967-5237

References

- 1. K. Zhang, X. P. Han, Z. Hu, X. L. Zhang, Z. L. Tao, and J. Chen, Chem. Soc. Rev.,
- 2. M. Huang, F. Li, F. Dong, Y. X. Zhang, and L. L. Zhang, J. Mater. Chem. A, 3, 21380 (2015).

- 3. G. P. Wang, L. Zhang, and J. J. Zhang, Chem. Soc. Rev., 41, 797 (2012).
- V. Subramanian, H. W. Zhu, R. Vajtai, P. M. Ajayan, and B. Q. Wei, J. Phys. Chem., 109, 20207 (2005).
- 5. C. J. Xu, F. Y. Kang, B. H. Li, and H. D. Du, J. Mater. Res., 25, 1421 (2010).
- F. Y. Cheng, J. Z. Zhao, W. Song, C. S. Li, H. Ma, J. Chen, and P. W. Shen, *Inorg.* Chem 45 2038 (2006)
- 7. J. X. Li, N. Wang, Y. Zhao, Y. H. Ding, and L. H. Guan, *Electrochem. Commun.*, 13, 698 (2011).
- X. Liu, C. Chen, Y. Zhao, and B. Jia, J. Nanomater., 2013, 736375 (2013).
- M. Xu and S. J. Bao, Energy Storage in the Emerging Era of Smart Grids, ed. R. Carbone (IntechOpen, London) p. 251 (2011).
- 10. W. B. Yan, J. Y. Kim, W. D. Xing, K. C. Donavan, T. Ayvazian, and R. M. Penner, Chem. Mater., 24, 2382 (2012).
- 11. L. Athouel, F. Moser, R. Dugas, O. Crosnier, D. Belanger, and T. Brousse, J. Phys. Chem. C, 112, 7270 (2008).
- 12. Q. Z. Zhang, D. Zhang, Z. C. Miao, X. L. Zhang, and S. L. Chou, Small, 14, 1702883 (2018).
- 13. R. Hausbrand, G. Cherkashinin, H. Ehrenberg, M. Groting, K. Albe, C. Hess, and W. Jaegermann, Mater. Sci. Eng. B. 192, 3 (2015).
- 14. P. Arora, R. E. White, and M. Doyle, *J. Electrochem. Soc.*, **145**, 3647 (1998).
- 15. J. Vetter, P. Novak, M. R. Wagner, C. Veit, K. C. Moller, J. O. Besenhard, M. Winter, M. Wohlfahrt-Mehrens, C. Vogler, and A. Hammouche, *J. Power* Sources, 147, 269 (2005).
- 16. F. Ataherian, K. T. Lee, and N. L. Wu, *Electrochim. Acta*, 55, 7429 (2010).
- 17. H. B. Tan, S. P. Wang, and X. R. Lei, J. Electrochem. Soc., 162, A448 (2015).
- 18. L. Yang, M. Takahashi, and B. F. Wang, Electrochim. Acta, 51, 3228 (2006).
- 19. M. R. Bailey and S. W. Donne, J. Electrochem. Soc., 159, A2010 (2012).
- 20. R. J. Gummow, A. Dekock, and M. M. Thackeray, Solid State Ionics, 69, 59 (1994). 21. J. Experton, X. J. Wu, G. L. Wang, and C. R. Martin, Chemelectrochem, 5, 3113 (2018).
- 22. C. R. Martin, M. Nishizawa, K. Jirage, and M. Kang, J. Phys. Chem. B, 105, 1925
- 23. V. P. Menon and C. R. Martin, Anal. Chem., 67, 1920 (1995).
- 24. C. R. Martin, Science, 266, 1961 (1994).
- 25. J. Experton and C. R. Martin, Small, 14, 1703290 (2018).
- 26. P. Dejardin, E. N. Vasina, V. V. Berezkin, V. D. Sobolev, and V. I. Volkov, Langmuir, 21, 4680 (2005).
- 27. P. Apel, Radiat. Meas., 34, 559 (2001).
- 28. J. Experton, A. G. Wilson, and C. R. Martin, *Anal. Chem.*, **88**, 12445 (2016).
- 29. P. Gao and C. R. Martin, ACS Nano, 8, 8266 (2014).
- 30. M. Y. Timmermans, N. Labyedh, F. Mattelaer, S. P. Zankowski, S. Deheryan, C. Detavernier, and P. M. Vereecken, J. Electrochem. Soc., 164, D954 (2017).
- 31. A. Biswal, B. C. Tripathy, K. Sanjay, T. Subbaiah, and M. Minakshi, RSC Adv., 5, 58255 (2015).
- 32. W. B. Yan, T. Ayvazian, J. Kim, Y. Liu, K. C. Donavan, W. D. Xing, Y. G. Yang, J. C. Hemminger, and R. M. Penner, ACS Nano, 5, 8275 (2011).
- 33. F. Grote and Y. Lei, *Nano Energy*, 10, 63 (2014).
- 34. D. W. Liu, Q. F. Zhang, P. Xiao, B. B. Garcia, Q. Guo, R. Champion, and G. Z. Cao, Chem. Mater., 20, 1376 (2008).
- 35. J. Experton, X. J. Wu, and C. R. Martin, Nanomaterials, 7, 445 (2017).
- 36. T. Shen, Y. Liu, Y. Zhu, D. Q. Yang, and E. Sacher, Appl. Surf. Sci., 411, 411 (2017)
- 37. A. Doren, M. J. Genet, and P. G. Rouxhet, Surf. Sci. Spectra, 3, 337 (1994).
- 38. M. Toupin, T. Brousse, and D. Belanger, Chem. Mater., 14, 3946 (2002).
- 39. M. Minakshi, P. Singh, T. B. Issa, S. Thurgate, and R. De Marco, J. Power Sources, 153, 165 (2006).
- 40. J. Song, J. Duay, E. Gillette, and S. B. Lee, Chem. Commun., 50, 7352 (2014).
- 41. L. Z. Wang, Y. Omomo, N. Sakai, K. Fukuda, I. Nakai, Y. Ebina, K. Takada, M. Watanabe, and T. Sasaki, Chem. Mater., 15, 2873 (2003).
- 42. R. Chromik and F. Beck, *Electrochim. Acta*, 45, 2175 (2000).
- 43. M. Le Thai, G. T. Chandran, R. K. Dutta, X. W. Li, and R. M. Penner, ACS Energy Lett., 1, 57 (2016).
- 44. A. S. Etman, A. Radisic, M. M. Emara, C. Huyghebaert, and P. M. Vereecken, J. Phys. Chem. C, 118, 9889 (2014).
- 45. S. Franger, S. Bach, J. P. Pereira-Ramos, and N. Baffier, J. Electrochem. Soc., 147, 3226 (2000).
- 46. S. C. Pang and M. A. Anderson, J. Mater. Res., 15, 2096 (2000).
- 47. D. Bélanger, T. Brousse, and J. W. Long, Electrochem. Soc. Interface, 17, 49 (2008)
- 48. E. Preisler, J. Appl. Electrochem., 6, 311 (1976).
- C. Monroe and J. Newman, *J. Electrochem. Soc.*, **150**, A1377 (2003).
 X. Wang, W. Zeng, L. Hong, W. W. Xu, H. K. Yang, F. Wang, H. G. Duan, M. Tang, and H. Q. Jiang, Nat. Energy, 3, 227 (2018).
- 51. R. M. Penner, J. Phys. Chem. B, 105, 8672 (2001).
- 52. R. V. Magan, R. Sureshkumar, and B. Lin, J. Phys. Chem. B, 107, 10513 (2003).
- 53. H. Kim, J. Hong, K. Y. Park, S. W. Kim, and K. Kang, Chem. Rev., 114, 11788